

A GPU-friendly Geometric Data Model and Algebra for Spatial Queries: Extended Version

Harish Doraiswamy and Juliana Freire

New York University

harishd@nyu.edu

juliana.freire@nyu.edu

Abstract

The availability of low cost sensors has led to an unprecedented growth in the volume of spatial data. However, the time required to evaluate even simple spatial queries over large data sets greatly hampers our ability to interactively explore these data sets and extract actionable insights. Graphics Processing Units (GPUs) are increasingly being used to speedup spatial queries. However, existing GPU-based solutions have two important drawbacks: they are often tightly coupled to the specific query types they target, making it hard to adapt them for other queries; and since their design is based on CPU-based approaches, it can be difficult to effectively utilize all the benefits provided by the GPU. As a first step towards making GPU spatial query processing mainstream, we propose a new model that represents spatial data as geometric objects and define an algebra consisting of GPU-friendly composable operators that operate over these objects. We demonstrate the expressiveness of the proposed algebra by formulating standard spatial queries as algebraic expressions. We also present a proof-of-concept prototype that supports a subset of the operators and show that it is at least two orders of magnitude faster than a CPU-based implementation. This performance gain is obtained both using a discrete Nvidia mobile GPU and the less powerful integrated GPUs common in commodity laptops.

1 Introduction

The availability of low cost sensors such as GPS in vehicles, mobile and IoT devices have led to an unprecedented growth in the volume of spatial data. Extracting insights from these data sets requires the ability to effectively and efficiently handle a variety of queries.

The most common approach to support spatial queries is through the use of spatial extensions that are available in existing relational database systems (e.g., the PostGIS extension for PostgreSQL [38], Oracle Spatial [32], DB2 Spatial Extender [1], SQL Server Spatial [44]). Popular geographic information system (GIS) software typically use these systems to process spatial queries [4, 19, 39] and some also provide their own database backend. Using these state-of-the-art systems, the response times to even simple spatial queries over large data sets can run into several minutes (or more), hampering the ability to perform interactive analytics over these data [15, 29]. While faster response times can be attained by powerful clusters [14, 34], such an option, due to its costs and complexity, is often out of reach for many analysts.

Recent technological advances have made Graphics Processing Units (GPUs) a cost-effective alternative to provide high computing power. Since GPUs are widely available, even in commodity laptops, effective GPU-based solutions have the potential to democratize large-scale spatial analytics. Not surprisingly, several approaches have been proposed that use GPUs to speed up spatial queries (e.g., [10, 11, 53–55]). However, these implementations typically follow the traditional approaches that were designed primarily for the CPU,

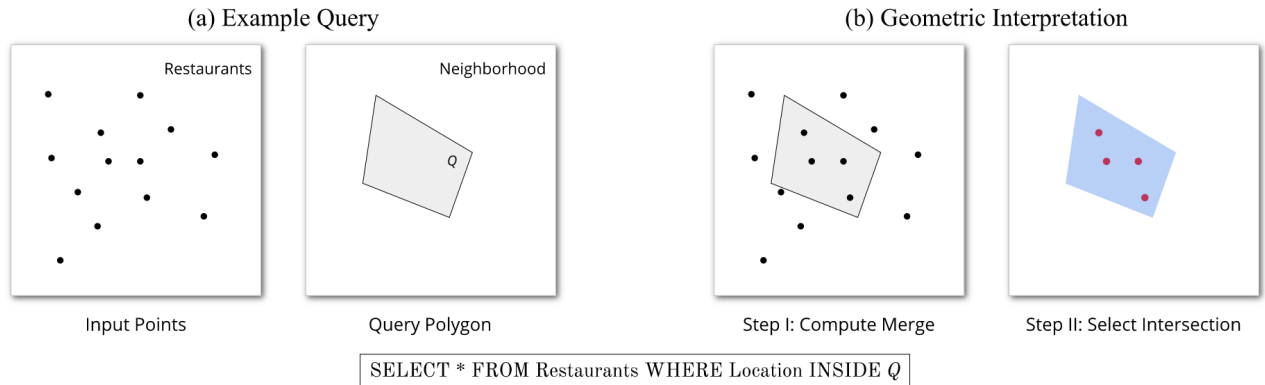


Figure 1: Reformulation of the spatial selection query.

and simply porting the algorithms may lead to an ineffective use of GPU capabilities. For example, a spatial aggregation query that aggregates input points across different polygonal regions would typically be implemented as a spatial join of the points and polygons followed by the aggregation of the join results. On the other hand, the recently proposed RasterJoin [47] represented a departure from traditional strategies: by modeling spatial aggregation queries using GPU-specific operations, it attained significant speedups even over the traditional query plan executed on a GPU, suggesting that GPU-specific strategies can lead to substantial performance gains.

Another drawback of traditional GPU-based approaches is that they require different implementations for each query class. Consequently, it is hard to re-use and/or extend them for other similar queries. As an example, consider the simple spatial selection query illustrated in Figure 1(a). Given a spatial data set consisting of a collection of points (say restaurants) and their locations, this query identifies all points that are contained within the specified query polygon (e.g., a neighborhood). Existing approaches (including the state-of-the-art GPU-based solution [11]) implement this query as a single operator typically making use of a spatial index, which organizes the minimum bounding rectangle (MBR) of the spatial objects in a tree structure. The index is used to identify relevant MBRs, and then, for each point inside the selected MBRs, a test is performed to check whether the point is indeed inside the query polygon. Note that this containment test is specific to the input being points. If the spatial component of the data is instead represented as the polygon corresponding to the land plot where the restaurant is located, the selection query requires a different implementation, since a polygon-intersect-polygon test must be performed instead. This shortcoming, coupled with the complexities involved in implementing GPU-based solutions, has impeded a wider use of GPUs in spatial databases.

Our Approach. With the goal of enabling GPUs to be exploited without the need to build custom solutions, we revisit the problem of designing a spatial data model and operators. We adapt common computer graphics operations for which GPUs are specifically designed and optimized, to propose a *new geometric data model that provides a uniform representation for different geometric objects*, and an *algebra consisting of a small set of composable operators capable of handling a wide variety of spatial queries*.

While several data models and algebras have been described in the literature [12, 18, 20, 22, 42], they were all designed before the advent of modern GPUs and suffer from at least one of the above shortcomings, as we discuss in Section 8. Furthermore, these models are typically *user-facing*: users express the queries of interest by making use of the data types and the operators provided in the model; the implementation of the operators is left to the developer. In contrast, we aim for a *developer-facing* model that can be incorporated into existing systems unbeknownst to the users, while at the same time providing significant benefits to the database engine and query performance.

To give an intuition behind the proposed geometric model, consider again the example in Figure 1(a) from a geometric point of view. The query can be translated into two operations performed one after the other

as shown in Figure 1(b). Visually (or graphically), the input points and the query polygon are uniformly represented as *drawings on a canvas*. The first operation merges the input points and the query polygon into a single canvas. The second operation computes the intersection between the points and the polygon to eliminate points outside the polygon. Unlike the traditional execution strategy for spatial aggregation (i.e., join followed by aggregation), the two operations used here are applicable to any kind of geometry. Therefore, even if the data (restaurants) were represented as polygons instead of points, the same set of operations could be applied.

Informally, we represent a spatial object as an embedding of its geometry onto a plane, called a *canvas*, and define GPU-friendly operators similar to the ones in Figure 1(b), that act on one or more canvases. As we show in Section 4, these operators can be re-used and composed to support a diverse set of spatial queries.

Given a small set of basic operators, our model makes it possible for implementations to focus on the efficiency of these operators, the gains from which become applicable to a variety of queries. While our focus in this paper is on the conceptual representation and modeling of spatial data and the design of the algebra, this work opens new avenues for research in spatial query optimization, both for theory (e.g., developing plan generation strategies, designing cost models) and systems (e.g., designing indexes leveraging GPUs).

Contributions. To the best of our knowledge, this is the first approach to propose a query algebra designed with a focus on enabling an efficient GPU realization of spatial queries. Our main contributions are as follows:

- We propose a new geometric data model that provides a uniform representation for spatial data on GPUs (Section 2).
- We design a spatial algebra consisting of five fundamental operators designed based on common computer graphics operations (Section 3). We show that the algebra is: expressive and able to represent all standard spatial queries; and closed, allowing the operators to be composed to construct complex queries (Section 4).
- We present a proof-of-concept implementation of a subset of the proposed operators that shows: 1) how the proposed model and operators are naturally suited for GPUs; and 2) how operators can be re-used in different queries. Our implementation achieves over two orders of magnitude speedup over a custom CPU-based implementation, and outperforms custom GPU-based approaches (Sections 5 & 6).
- We discuss the compatibility of the proposed algebra with the relational model and its utility for query optimization (Section 7).

2 Data Representation

In this section, we first formalize the notion of a spatial data set, and then define the concept of a *canvas*, the spatial analogue of a relational tuple.

2.1 Spatial Data

As discussed in Section 1, an important limitation of current spatial operations is that they are tied to specific representations for geometric data types. To design flexible operators, we need a uniform representation for the geometry that is independent of underlying types. We propose to schematically represent the geometry using a single type called *geometric object*, which can conceptually represent any complex geometric structure.

Definition 1 (Geometric Object) *A geometric object is defined as a collection of geometric primitives.*

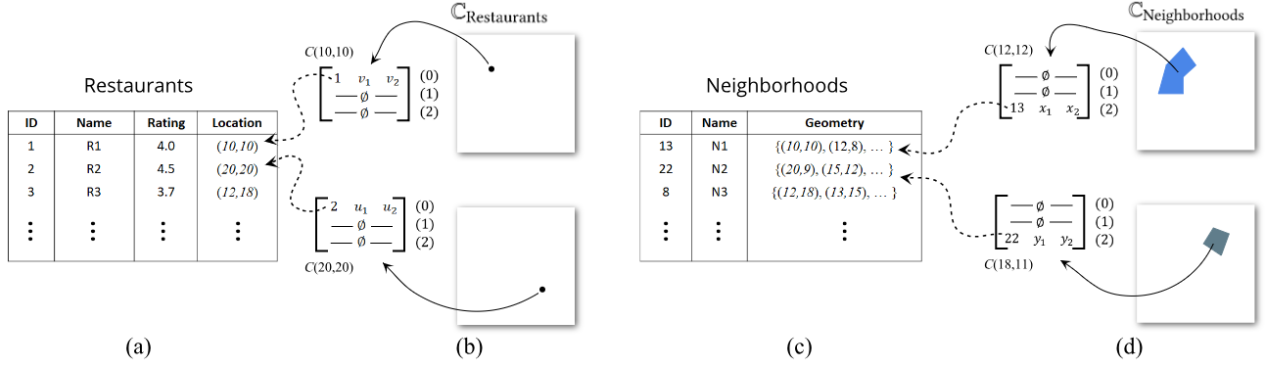


Figure 2: *Canvas*: A uniform representation of spatial data. (a) Example point data. (b) Two canvases corresponding to the first two records of the table. The [0,0] element of the matrix (corresponding to the 0-primitive) stores the unique ID corresponding to the record. (c) Example polygon data. (d) Two canvases corresponding to the first two records. Here, all points inside a polygon will map to the same value, with the element [2,0] (corresponding to the 2-primitives) storing the unique ID. The white parts of the canvas (not part of the geometry) maps to a null value.

Definition 2 (Geometric Primitive) A d -dimensional geometric primitive (d -primitive) is defined as a d -manifold (with or without a boundary).

Informally, a d -manifold is geometric space in which the local neighborhood of every point represents \mathbb{R}^d . In the context of spatial data that is of interest in this work, we focus on 2-dimensional (2D) space and d -primitives, where $0 \leq d \leq 2$. Intuitively, a 0-primitive is a point while a 1-primitive is a line (not necessarily a straight line or with a finite length). 2-primitives include any subset of \mathbb{R}^2 that is neither a line nor a point, such as polygons and half spaces.

A spatial data set can now be defined in terms of geometric objects as follows:

Definition 3 (Spatial Data) A spatial data set consists of one or more attributes of type geometric object.

Note that the above definition allows geometric objects of arbitrarily complex shapes composed using a heterogeneous set that contains points, lines, as well as polygons. However, geometric objects common in real world data sets are primarily only points (e.g., locations of restaurants, hospitals, bus stops, etc.), only lines (e.g., road networks), or only polygons (e.g., state or city boundaries).

2.2 Canvas

We define the notion of a canvas to explicitly capture the geometric structure of a spatial data set. As mentioned above, we assume that the dimensions of the geometric primitives composing a geometric object in a spatial data set is either 0, 1 or 2. Let S be a set of k -tuples, where $k \geq 1$, such that $\emptyset \in S$. A *canvas* is formally defined as follows:

Definition 4 (Canvas) A canvas is a function $C : \mathbb{R}^2 \rightarrow S^3$ that maps each point in \mathbb{R}^2 to a triple $(s[0], s[1], s[2]) \in (S \times S \times S)$, where the i^{th} element of the triple, $s[i]$, stores information (as a k -tuple) corresponding to i -dimensional geometric primitives.

Definition 5 (Empty Canvas) A canvas C is empty iff C maps all points in \mathbb{R}^2 to $(\emptyset, \emptyset, \emptyset)$.

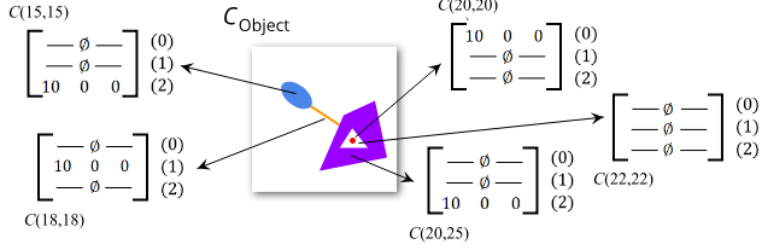


Figure 3: A canvas representing a complex object. Since all the primitives (colored differently) are part of the same object, they have the same ID.

A canvas is analogous to a tuple in the relational model. It is defined such that it captures geometric objects in the world coordinate space of the graphics pipeline, thus making it straightforward to apply computer graphics operations on it. Intuitively, a canvas stores for each point in \mathbb{R}^2 information corresponding to the geometric primitives that pass through that point. This information is captured by the elements of the set S (we discuss S in more detail below).

Given a spatial data set, each record of this data is represented using one or more canvases equal to the number of geometric object attributes of the data. For ease of exposition, consider a spatial data set having a single geometric object attribute and a geometric object o corresponding to one of the records in this data. Let $o = \{g_1, g_2, g_3, \dots, g_n\}$, where g_i is a geometric primitive having dimension $\dim(g_i)$, $0 \leq \dim(g_i) \leq 2$, $\forall i$. A canvas representation of the geometric object o is defined as follows.

Definition 6 (*Canvas representation of a geometric object*) A canvas corresponding to a geometric object is a function $C_o : \mathbb{R}^2 \rightarrow S^3$ such that $\forall d \in [0, 2]$

$$C_o(x, y)[d] = \begin{cases} s_d \neq \emptyset \in S, & \text{if } \exists i \mid \dim(g_i) = d \text{ and} \\ & g_i \text{ intersects } (x, y) \\ \emptyset & \text{otherwise} \end{cases}$$

The set S used in the above definition is called the *object information set*, and is defined as follows.

Definition 7 (*Object Information Set S*) The object information set S is defined as a set of triples (v_0, v_1, v_2) where v_0 stores a unique identifier (or a pointer) for the record corresponding to the geometric object. v_1 and v_2 are real numbers storing meta data related to the canvas.

The range of the canvas function C can thus be represented as a 3×3 matrix, where each row corresponds to the Object Information Set for the associated primitive dimension. We abuse notation to represent the triple $(\emptyset, \emptyset, \emptyset)$ simply as \emptyset .

Example 1: Consider the two example data sets in Figure 2. The first data set corresponds to the set of restaurants in a city (represented as points) (a), while the second data set corresponds to the neighborhood boundaries of this city (represented as polygons) (c). Figure 2 also illustrates the canvas representations corresponding to two records from each of these two data sets. Note that in this example, we use only the identifier element of the object information set. The values of the other elements are initialized depending on the query scenario (Section 4).

Example 2: The complex geometric object shown in Figure 3 consists of two polygons (an ellipse and a polygon with a hole) connected by a line, with the hole also containing a point. This is represented in the canvas by mapping the regions corresponding to the different primitives using the appropriate rows in the matrix (for point, line, polygon).

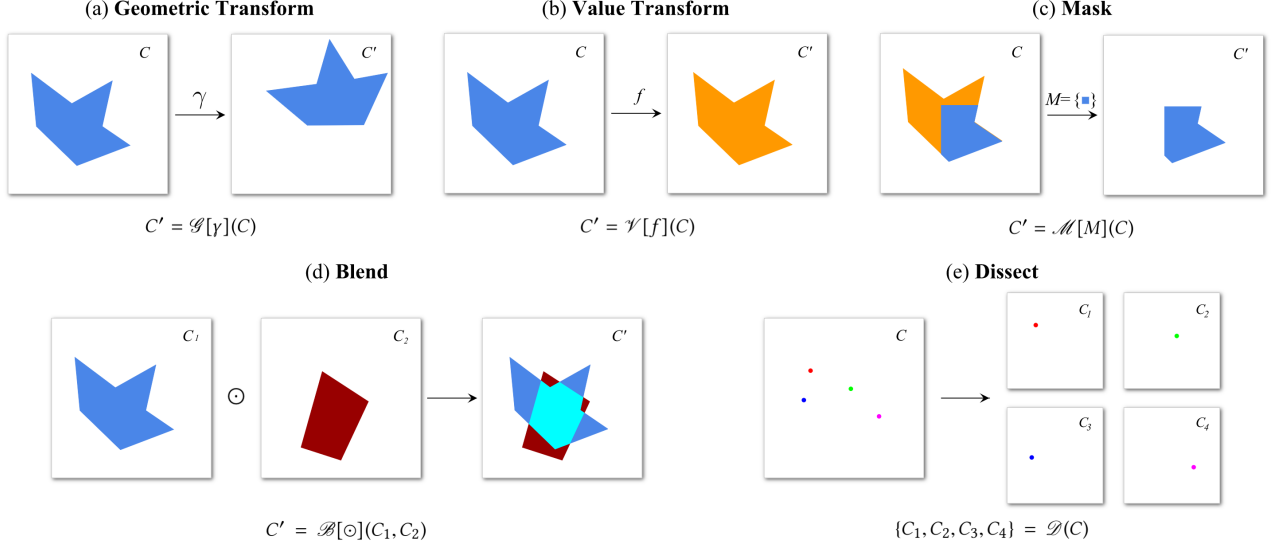


Figure 4: The 5 fundamental operators. For illustrative purposes, we use colors to denote the information stored in each point of the canvas; the white color corresponds to a null value.

3 Operators

Below, we define the operators we designed for the canvas representation of a spatial data set. Concrete examples of how these operators are used are given in Section 4. We categorize the set of operators into three classes: fundamental, derived, and utility operators. We use the following notation to represent operators that take as input zero or more canvases:

$$Op[P_1, P_2, \dots](C_1, C_2, \dots, C_n)$$

where Op is the operator name, $P_i, \forall i$, the parameters of the operator, and $C_j, \forall j$, the canvases input to the operator. The output of all the operators is always one or more canvases. Thus, *the proposed algebra is closed by design*.

3.1 Fundamental Operators

Fundamental operators form the core of the proposed algebra. Their design is based on common computer graphics operations that are already supported in GPUs. Figure 4 illustrates the five fundamental operators.

Geometric Transform $C' = \mathcal{G}[\gamma](C)$: This operator takes as input a single canvas C and outputs a canvas C' in which all the geometric objects of C are transformed to a new position in C' defined by the parameter function γ . Here, the parameter function γ can be defined in two ways:

1. $\gamma : \mathbb{R}^2 \rightarrow \mathbb{R}^2$
2. $\gamma : S^3 \rightarrow \mathbb{R}^2$

In the first case, the new position (x', y') of a geometry is dependent on its current position (x, y) :

$$C'(\gamma(x, y)) = C(x, y)$$

Examples of such functions include operations such as rotation, translation, etc. The example in Figure 4(a) rotates and translates (moves) the polygon object to a different position.

A scenario where this operator is useful is when spatial data sets in a database use different coordinate systems. Thus, when performing binary or n-ary operations on canvases from these data sets, the geometry has to be converted into a common coordinate system first. The parameter function γ can be defined appropriately for this purpose.

In the second case, the new position (x', y') of the geometry is dependent on the information stored at the current position $C(x, y)$:

$$C'(\gamma(C(x, y))) = C(x, y)$$

Such a transformation is useful, for example, when one is interested in accumulating values (e.g., for aggregation queries) corresponding to a geometric object—in this case, the function γ can be defined to move all points having the same object identifier to a unique location.

Value Transform $C' = \mathcal{V}[f](C)$: This unary operator outputs a canvas C' in which the information corresponding to the geometries is modified based on the parameter function f . That is,

$$C'(x, y) = f(x, y, C(x, y))$$

where, $f : \mathbb{R}^2 \times S^3 \rightarrow S^3$ is a function that changes the object information based on its location and/or value. Figure 4(b) illustrates an example of this operation where the color of the polygon in the canvas is changed from blue to orange.

Mask $C' = \mathcal{M}[M](C)$: The mask operator is used to filter regions of canvas so that only regions satisfying the condition specified by $M \subset S^3$ are retained. Formally, the application of this operator results in the canvas C' such that

$$C'(x, y) = \begin{cases} C(x, y), & \text{if } C(x, y) \in M \\ \emptyset & \text{otherwise} \end{cases}$$

For example, this can be used to accomplish select intersection operations shown in Figure 1(b) and Figure 4(c).

Blend $C' = \mathcal{B}[\odot](C_1, C_2)$: Blend is a binary operator used to merge two canvases into one. The blend function $\odot : S^3 \times S^3 \rightarrow S^3$ defines how the merge is performed:

$$C'(x, y) = C_1(x, y) \odot C_2(x, y)$$

The merge operation used in Figure 1(b) is an instance of the blend function. Another example is shown in Figure 4(d).

Dissect $\{C_1, C_2, \dots, C_n\} = \mathcal{D}(C)$: The dissect operation splits a given canvas into multiple non-empty canvases, each corresponding to a point $(x, y) \in \mathbb{R}^2$ having $C(x, y) \neq \emptyset$. That is, a new canvas C_i is generated corresponding to a non-null point (x, y) such that

$$C_i(x', y') = \begin{cases} C(x, y), & \text{if } (x', y') = (x, y) \\ \emptyset & \text{otherwise} \end{cases}$$

For example, in Figure 4(e), a canvas encoding 4 points is split into 4 canvases each corresponding to one of those points. As we show later, one of the uses of this operator is for queries involving aggregations over geometries with 1- and 2-primitives (such as polygons).

3.2 Derived Operators

It is common for certain combinations of fundamental operators to be repeatedly used for various queries. We represent these combinations as derived operators and describe a couple of such useful operators below.

Multiway Blend $C' = \mathcal{B}^*[\odot](C_1, C_2, \dots, C_n)$: This n -ary operator takes as input n canvases and generates a single canvas after blending all these n canvases in the given order.

$$C' = \mathcal{B}[\odot](C_1, \mathcal{B}[\odot](C_2, \mathcal{B}[\odot](C_3, \dots)))$$

Note that if the blend function \odot is associative, then it allows relaxing the grouping of the different blend operations, thus providing more flexibility while optimizing queries.

Map $\{C_1, C_2, \dots, C_n\} = \mathcal{D}^*[\gamma](C)$: Map is a composition of a dissect followed by a geometric transform.

$$\{C_1, C_2, \dots, C_n\} = \mathcal{G}[\gamma](\mathcal{D}(C))$$

This operator is useful to align all the canvases resulting from the dissect. In such a case, γ is typically defined as a constant function:

$$\gamma(x, y) = (x_c, y_c)$$

where x_c and y_c are constants.

Without loss of generality, we assume the above notation of providing multiple canvases as input to a unary operator (in this case the geometric transform that takes as input canvases output from a dissect operation) as equivalent to applying the operator individually to each of the input canvases.

3.3 Utility Operators

Utility operators are primarily used to generate canvases based on a set of parameters. These are particularly useful for classes of spatial queries involving parametric constraints. In particular, we consider the following three types of utility operators:

Circle $C = \text{Circ}[(x, y), r]()$: generates a canvas corresponding to a circle with center is (x, y) and radius r .

Rectangle $C = \text{Rect}[l_1, l_2]()$: generates a canvas corresponding to a rectangle having diagonal end points l_1 and l_2 .

Half Space $C = \text{HS}[a, b, c]()$: generates a canvas representing the half space defined by the equation: $ax + by + c < 0$.

4 Expressiveness

To demonstrate the expressiveness of the proposed model, in what follows we describe how common spatial queries can be represented as algebraic expressions. We build upon the classification of spatial queries used by Eldawy et al. [14] and categorize spatial queries into the following classes: *selection*, *join*, *aggregate*, *nearest neighbor*, and *geometric queries*. Note that this is a super set of the query types evaluated in a state-of-the-art experimental survey by Pandey et al. [34].

For ease of exposition, we consider only point and polygonal data sets. It is straightforward to express similar queries for other types of spatial data sets with lines, or more complex geometries (combination of points, lines and polygons). Without loss of generality, we assume that the different operators prune empty canvases from their output, and an empty canvas is generated when an input canvas does not satisfy a given constraint. This is similar to the relational model, where tuples that do not match the query constraints are excluded from the output table.

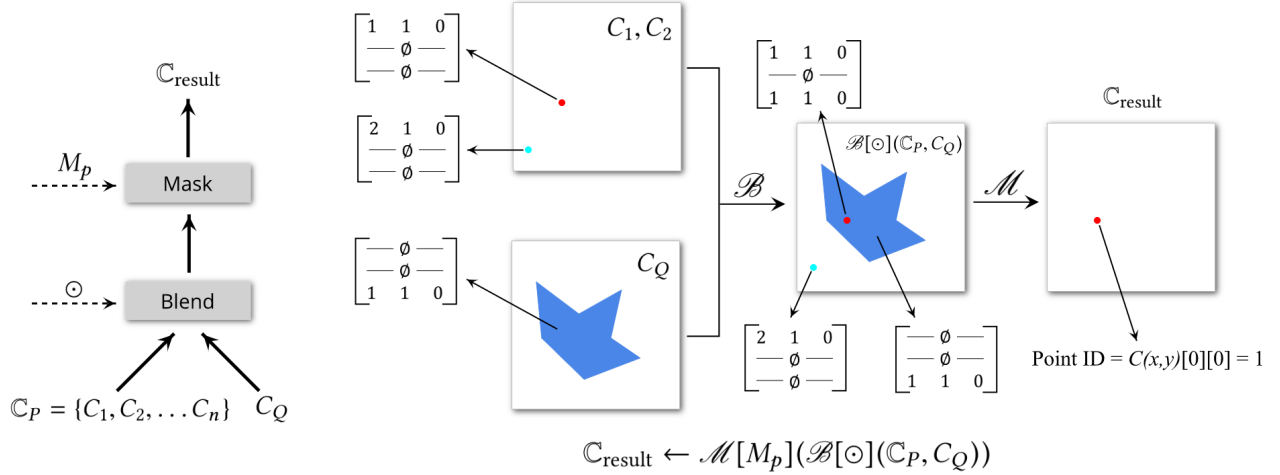


Figure 5: A schematic representation as a plan diagram of the algebraic expression used to select points based on a polygonal constraint (left). The different steps of this plan is illustrated using an example input with 2 points (colored red and cyan)(right). For simplicity, both points are shown in a single canvas.

4.1 Selection Queries

We can classify spatial selection queries into three types: polygonal selection, range selection, and distance-based selection.¹ We first consider selection queries that have a polygonal constraints, and then extend the algebraic expressions for other types of selection queries.

Polygonal Selection of Points. Let D_P be a data set consisting of a set of points. Let $\{(x_1, y_1), (x_2, y_2), \dots, (x_n, y_n)\}$ be the coordinates corresponding to the location of these points. Let Q be any arbitrary-shaped polygon. Consider the following spatial query expressed in an SQL-like syntax:

SELECT * FROM D_P WHERE Location INSIDE Q

Note that this is the same query used for the example in Figure 1(a). Using the proposed data representation, let $C_P = \{C_1, C_2, \dots, C_n\}$ be the set of canvases corresponding to each point (record) in D_P . Let the canvas C_i corresponding to the i^{th} record be defined as follows:

$$\begin{aligned}
 C_i(x, y)[0] &= \begin{cases} (id, 1, 0) & \text{if } (x, y) = (x_i, y_i) \\ \emptyset & \text{otherwise} \end{cases} \\
 C_i(x, y)[1] &= \emptyset \\
 C_i(x, y)[2] &= \emptyset
 \end{aligned}$$

Here, id corresponds to the unique identifier mapping the canvas to the corresponding record in D_P . We use the second element of the tuple $C_i(x, y)[0]$ to keep count of the points incident on the location (x, y) , which in this case is 1. The third element is ignored for this query. Let the canvas C_Q corresponding to the query polygon Q be defined as follows:

$$\begin{aligned}
 C_Q(x, y)[0] &= \emptyset \\
 C_Q(x, y)[1] &= \emptyset \\
 C_Q(x, y)[2] &= \begin{cases} (1, 1, 0) & \text{if } (x, y) \text{ falls inside } Q \\ \emptyset & \text{otherwise} \end{cases}
 \end{aligned}$$

¹While nearest-neighbor-based selection could also be in this category, we place it in a separate class (Section 4.4).

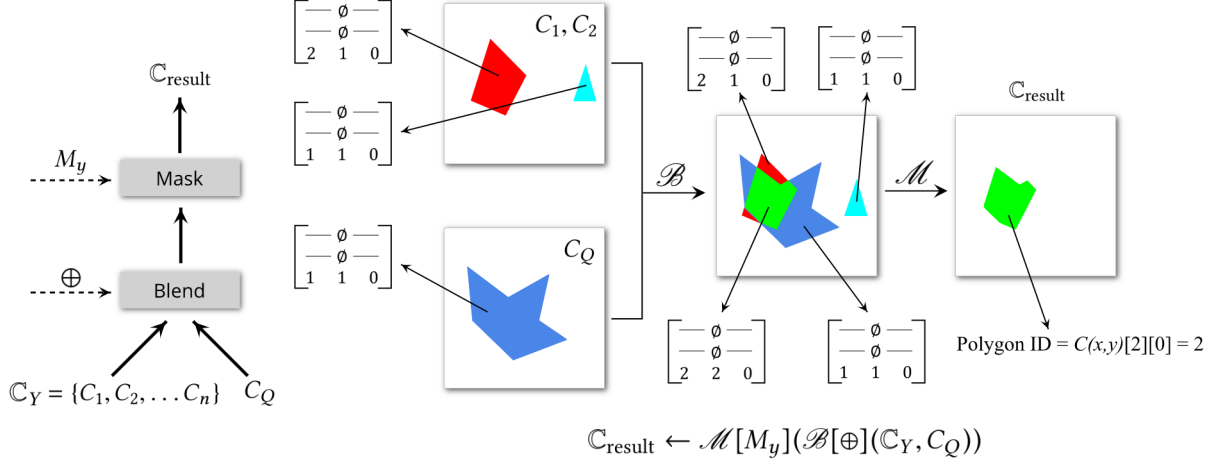


Figure 6: Plan diagram corresponding to the algebraic expression used to select polygons based on a polygonal constraint (left). This plan is illustrated using 2 input polygons (colored red and cyan) (right), which are shown in a single canvas.

Similar to the case of points above, the elements $C_Q(x, y)[2][0]$ and $C_Q(x, y)[2][1]$ stores the *id* of the query polygon (set to 1 since there is only one polygon) and count of 2-primitives incident on (x, y) respectively. Using the canvases defined above, the select query can be algebraically expressed as follows:

$$C_{\text{result}} \leftarrow \mathcal{M}[M_p](\mathcal{B}[\odot](C_P, C_Q))$$

where, $\forall s_1, s_2 \in S^3$

$$s_1 \odot s_2 = \begin{bmatrix} s_1[0][0] & s_1[0][1] & s_1[0][2] \\ \text{---} & \emptyset & \text{---} \\ s_2[2][0] & s_2[2][1] & s_2[2][2] \end{bmatrix}$$

and

$$M_p = \{s \in S^3 \mid s[0] \neq \emptyset \text{ and } s[2][0] = 1\}$$

Similar to the example in Figure 1(b), the above expression first merges the input data with the query polygon using the blend operator \mathcal{B} , and then uses the mask operator \mathcal{M} to select only the intersection (a location is part of the intersection if both, a 1-primitive and 2-primitive are incident on it). Figure 5 visualizes the above expression as a plan diagram, and illustrates the different steps for two examples when a point is inside the query polygon (and hence part of the result), and when a point is outside respectively.

Polygonal Selection of Polygons. Let D_Y be a data set consisting of a set of polygons. Let $\{Y_1, Y_2, \dots, Y_n\}$ be the set of polygons associated with each record of the data set. As before, the polygons can take any shape. Let Q be another arbitrary-shaped polygon.

Let the set of canvases C_Y corresponding to polygons in D_Y be defined as follows:

$$\begin{aligned} C_i(x, y)[0] &= \emptyset \\ C_i(x, y)[1] &= \emptyset \\ C_i(x, y)[2] &= \begin{cases} (id, 1, 0) & \text{if } (x, y) \text{ falls inside } Y_i \\ \emptyset & \text{otherwise} \end{cases} \end{aligned}$$

Let the canvas corresponding to query polygon Q be defined as before. Now, consider the following selection query, similar to the one above, but over D_Y :

`SELECT * FROM DY WHERE Geometry INTERSECTS Q`

This query can be algebraically expressed as follows:

$$\mathbb{C}_{\text{result}} \leftarrow \mathcal{M}[M_y](\mathcal{B}[\oplus](\mathbb{C}_Y, C_Q))$$

where, $\forall s_1, s_2 \in S^3$

$$s_1 \oplus s_2 = \begin{bmatrix} \text{---} & \emptyset & \text{---} \\ \text{---} & \emptyset & \text{---} \\ s_1[2][0] & s_1[2][1] + s_2[2][1] & s_1[2][2] \end{bmatrix}$$

and

$$M_y = \{s \in S^3 \mid s[2][1] = 2\}$$

Note that unlike in the previous case of selecting points, since both the data as well as the query consist of polygons, both the data canvas and the query canvas store information only for 2-primitives. Hence, the second element of the information tuple is made use of in this case to compute the intersection (i.e., locations having two 2-primitives incident on them). Figure 6 shows the algebraic expression using a plan diagram, and illustrates two examples denoting selection and non-selection scenarios respectively.

Selection Using Other Spatial Constraints. In addition to polygonal constraints, selection queries over spatial data may also involve other types of spatial constraints. Commonly used are range constraints and distance-based selection. It is easy to extend the algebraic expressions used for polygonal constraints to these scenarios as follows.

1. *Rectangular Range Constraints:* This class of queries requires the selection of spatial objects that intersect a 2D range. To execute such queries, the query polygon is simply replaced by a rectangle, the canvas for which can be created using the utility operator: $C_Q \leftarrow \text{Rect}[l_1, l_2]()$, where l_1, l_2 denotes the diagonal endpoints of the rectangle range.

2. *One-Sided Range Constraints:* In this scenario, the queries require selecting geometries that intersect a given half-space $ax + by + c < 0$ (note that this is a more generic formulation of queries involving constraints such as $x < c$ or $y < c$). Again, the utility operator can be used to generate the required query canvas as a replacement for the query polygon:

$$C_Q \leftarrow \text{HS}[a, b, c]()$$

3. *Distance-based Selection:* In this case, the queries require the selection of geometries that lie within a given distance d of a query point (x_q, y_q) . This essentially translates to using a circle with radius d centered at (x_q, y_q) as the query polygon, the canvas for which can also be created using the utility operator: $C_Q \leftarrow \text{Circ}[(x_q, y_q), d]()$

Given the possibility to adapt these three types of spatial constraints to a polygon, we will focus only on polygonal constraints for the remainder of this section.

4.2 Join Queries

Spatial join queries can be broadly classified into three types: (Type I) points \bowtie polygons join; (Type II) polygons \bowtie polygons join; and (Type III) points \bowtie points join. Type III is commonly known as a distance join. As in the previous section, one set of points (say the RHS) of the distance join can be converted into a collection of circles to transform this to a points \bowtie polygons join query. We therefore focus on the first two types of join queries.

Let D_P and D_Y be a point data set and a polygon data set respectively. A Type I join query between these two data sets is typically specified as follows:

<code>SELECT * FROM D_P, D_Y WHERE D_P.Location INSIDE D_Y.Geometry</code>
--

Similarly, let D_{Y_1} and D_{Y_2} be two polygon data sets. A Type II join query between these two data sets can be specified as follows:

```
SELECT * FROM DY1, DY2 WHERE DY1.Geometry INTERSECTS DY2.Geometry
```

The above join queries are equivalent to performing selection queries, one for each record (canvas) from D_Y and D_{Y_2} respectively. Thus, conceptually, the algebraic expression for joins is the same as the corresponding selection queries, with the exception that a single query polygon is instead replaced with a collection of polygons. A Type I join query can then be realized using the following expression

$$C_{\text{result}} \leftarrow \mathcal{M}[M_p](\mathcal{B}[\odot](C_P, C_Y))$$

while a Type II join query can be realized using

$$C_{\text{result}} \leftarrow \mathcal{M}[M_y](\mathcal{B}[\oplus](C_{Y_1}, C_{Y_2}))$$

Here, C_P , C_Y , C_{Y_1} , and C_{Y_2} are collections of canvases corresponding to the data sets D_P , D_Y , D_{Y_1} and D_{Y_2} respectively. The different parameters of the operators in the above expressions remain the same as what was used for their selection counterparts.

Similar to the join operator in the relational model, spatial joins using our model can be implemented in several ways. A straightforward approach is using nested loops for the blend operation, which can be made more efficient if spatial indexes are available.

4.3 Aggregate Queries

The third class of queries common for spatial data are spatial aggregation queries. We consider two types of such queries: aggregating the results from a selection, and the aggregation required for a group-by over a join.

Aggregation over a Select. Consider first a simple count of the results from a selection query:

```
SELECT COUNT(*) FROM DP WHERE Location INSIDE Q
```

This query can be realized using the expression:

$$C_{\text{count}} \leftarrow \mathcal{B}^*[+](\mathcal{G}[\gamma_c](C_{\text{result}}))$$

where $\gamma_c : S^3 \rightarrow \mathbb{R}^2$ is defined such that

$$\forall s \in S^3, \gamma_c(s) = (s[2][0], 0),$$

$+$: $S^3 \times S^3 \rightarrow S^3$ is defined as

$$s_1 + s_2 = \begin{bmatrix} 0 & s_1[0][1] + s_2[0][1] & 0 \\ - & \emptyset & - \\ s_2[2][0] & s_2[2][1] & s_2[2][2] \end{bmatrix}$$

and

$$C_{\text{result}} \leftarrow \mathcal{M}[M_p](\mathcal{B}[\odot](C_P, C_Q))$$

is the set of canvases resulting from the select operation (same as in Section 4.1 above).

Basically, each canvas (corresponding to a point) satisfying the selection constraint is transformed to a constant location $(1, 0)$ (recall that the *id* of the query polygon Q is 1), and the resulting canvases are merged together to compute the required summation (see Figure 7). The value of $C_{\text{count}}(1, 0)[0][1]$ stores the resulting count. Note that the second element of the tuple corresponding to the 0-primitives is used for this operation, while this was not necessary when performing only a select.

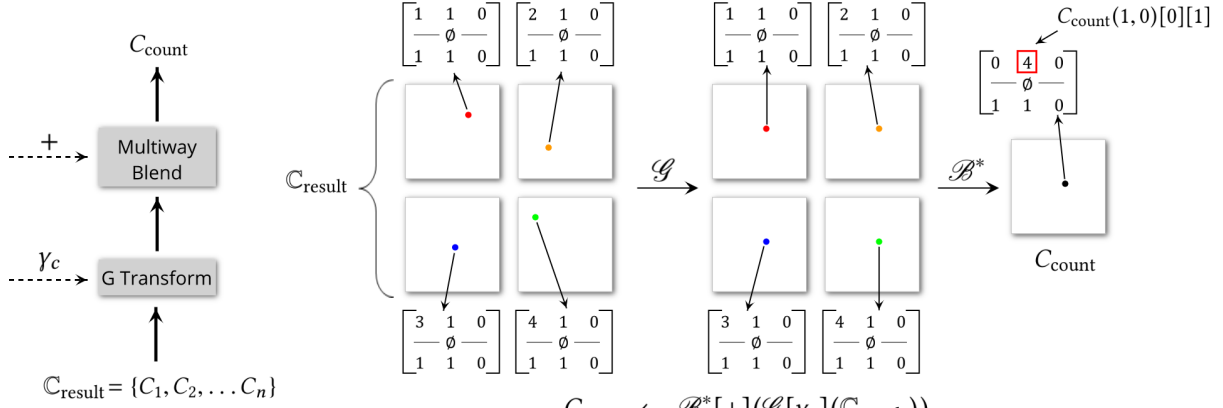


Figure 7: Plan diagram for aggregating the results from a select query (left). The example (right) uses the results from a select sub-query that returns 4 points, and illustrates the workflow that counts the results.

Instead of count, if the query requires computing other distributive (e.g., sum, minimum, maximum) or algebraic (e.g., average) aggregations over a given attribute, then the third element of the tuple corresponding to the 0-primitives can be used to store the value corresponding to this attribute, and the $+$ function can be modified appropriately. For example, let A be a real-valued attribute of the data set D_P . Consider the following query:

SELECT SUM(A) FROM D_P WHERE Location INSIDE Q

This query can be realized using the same expression as above by defining $C_i \in \mathbb{C}_P$ and $+$, respectively, as follows.

$$\begin{aligned}
 C_i(x, y)[0] &= \begin{cases} (id, 1, A[i]) & \text{if } (x, y) = (x_i, y_i) \\ \emptyset & \text{otherwise} \end{cases} \\
 C_i(x, y)[1] &= \emptyset \\
 C_i(x, y)[2] &= \emptyset \\
 s_1 + s_2 &= \begin{bmatrix} 0 & s_1[0][1] + s_2[0][1] & s_1[0][2] + s_2[0][2] \\ - & \emptyset & - \\ s_2[2][0] & s_2[2][1] & s_2[2][2] \end{bmatrix}
 \end{aligned}$$

In this scenario, the value of $C_{\text{result}}(1, 0)[0][2]$ maintains the required sum.

Aggregation over a Join. The second type of aggregation queries consist of a group-by operation over a spatial join. In particular, consider the following query:

SELECT COUNT(*) FROM D_P, D_Y WHERE D_P .Location INSIDE D_Y .Geometry
GROUP BY D_Y .ID

The algebraic expression used for aggregations over select works for this query as well:

$$C_{\text{count}} \leftarrow \mathcal{B}^*[+](\mathcal{G}[\gamma_c](C_{\text{result}}))$$

where

$$C_{\text{result}} \leftarrow \mathcal{M}[M_p](\mathcal{B}[\odot](C_P, C_Y))$$

When using the expression for a join, each of the polygons have a unique id . Hence, the join result corresponding to a point-polygon pair that satisfies the containment constraint will be moved to the location $(id, 0)$ corresponding to that polygon. Thus, the final multiway blend operation will individually count points within each of the polygons in D_Y . The value $C_{\text{count}}(id, 0)[0][1]$ stores the value corresponding to polygon with ID id .

4.4 Nearest-Neighbor Queries

We consider the following nearest-neighbor-based query template that finds the k points closest to a given query point $X(x_p, y_p)$ (k NN query).

```
SELECT * FROM  $D_P$  WHERE Location  $\in$  KNN( $X, k$ )
```

Without loss of generality, we assume that the distances of points in D_P to query point X are totally ordered, i.e., no two distances are the same. In the presence of a clash, the points can be perturbed by an infinitesimally small distance ϵ to ensure the total order condition is satisfied.

One way to answer this query is to first find the distance r such that there are exactly k points within the circle centered at X with radius r . Then, the distance-based selection can be used to obtain the query result. This workflow can be accomplished using the proposed algebra as follows. Let \mathbb{C}_X be a set of circles centered at X have increasing radii.² This can be accomplished by using the $Circ()$ utility operator. Let the id of each circle c be the radius of c . Then, the required radius r to identify the k nearest neighbors can be obtained using the following expression:

$$\mathbb{C}_r \leftarrow \mathcal{D}^*[\gamma_0](\mathcal{M}[M_r](C_{\text{count}})) \text{ where}$$

$$M_r = \{s \in S^3 \mid s[0][1] = k\}$$

$\gamma_0 : S^3 \rightarrow \mathbb{R}^2$ is defined as

$$\forall s \in S^3, \gamma_0(s) = (0, 0), \text{ and}$$

$$C_{\text{count}} \leftarrow \mathcal{B}^*[+](\mathcal{G}[\gamma_c](\mathcal{M}[M_p](\mathcal{B}[\odot](\mathbb{C}_P, \mathbb{C}_X))))$$

is the same join-group-by aggregation used above. Essentially, the *mask* operation is applied to the result from the aggregation to remove all circles containing fewer or more than k points, followed by a *map* to obtain individual canvases for each valid radius. Therefore, $C(0, 0)[2][0], \forall C \in \mathbb{C}_r$ has the *ids* of canvases corresponding to the circles having exactly k points in them. Since the *ids* correspond to the radius of the respective circles, this can then be used to perform a distance-based selection to complete the k NN query.

4.5 Computational Geometry Queries

The final class of queries we consider is the set of computational geometry queries. These include queries such as computing the Voronoi diagram, spatial skyline, and convex hull [14]. While it might not be straightforward to realize all of these queries algebraically, the provided operators can be used as part of a stored procedure to execute some of them.

We illustrate this through the following example: consider the query to compute the Voronoi diagram for a given set of points $\{(x_1, y_1), (x_2, y_2), \dots, (x_n, y_n)\}$. This can be accomplished using the following pseudo-code:

Procedure ComputeVoronoi

Require: Points $\{(x_1, y_1), (x_2, y_2), \dots, (x_n, y_n)\}$

- 1: $C_{\text{voronoi}} \leftarrow \emptyset$
 - 2: **for** each $i \in [1, n]$ **do**
 - 3: $C_{\text{voronoi}} \leftarrow \mathcal{V}[f_{(x_i, y_i)}](C_{\text{voronoi}})$
 - 4: **end for**
 - 5: **return** C_{voronoi}
-

²Conceptually there is an infinite number of circles, but in practice, a finite number of circles can be created with small increments in radii up to a maximum radius.

Here, $f_{(x_p, y_p)} : \mathbb{R}^2 \times S^3 \rightarrow S^3$ is defined as follows:

$$\begin{aligned} f_{(x_p, y_p)}(x, y, s)[0] &= \emptyset \\ f_{(x_p, y_p)}(x, y, s)[1] &= \emptyset \\ f_{(x_p, y_p)}(x, y, s)[2] &= \begin{cases} (i, d_2, 0) & \text{if } s = \emptyset \\ (s[2][0], s[2][1], 0) & s[2][1] < d_2 \\ (i, d_2, 0) & \text{otherwise} \end{cases} \end{aligned}$$

where d_2 is the Euclidean distance between the point (x, y) and the parameter point (x_p, y_p) . This procedure incrementally builds the Voronoi diagram by adding one input point at a time—during iteration i , the regions of existing polygons closest to point i are merged to form a new Voronoi region corresponding to this point.

It might not be possible to express all computational geometry queries as stored procedures using the previously defined operators. In such cases new operators can be added for such queries.

4.6 Complex Queries

So far we focused on standard queries and showed how they could be translated into algebraic expressions using the proposed algebra. As mentioned in Section 1, an algebra is useful only if the operators can be easily composed to also support more complex queries. In this section, we demonstrate this property using a spatial query involving constraints on two spatial attributes [16]: we consider selection queries over origin-destination data sets (e.g., taxi trips, migration data), where the selection is based on polygonal constraints on both origin as well as destination locations:

```
SELECT * FROM DP WHERE Origin INSIDE Q1 and Destination INSIDE Q2
```

Here, D_P is the input point data set having two location attributes *Origin* and *Destination*, and Q_1 and Q_2 are polygonal constraints over the two location attributes respectively. This query could be used, for example, to retrieve all the taxi trips between two specific neighborhoods.

Let \mathbb{C}_p be the canvases corresponding to D_P defined as before, but with respect to the origin attribute. Let C_{Q_1} and C_{Q_2} be canvases corresponding to the query constraints defined as follows:

$$\begin{aligned} C_{Q_i}(x, y)[0] &= \emptyset \\ C_{Q_i}(x, y)[1] &= \emptyset \\ C_{Q_i}(x, y)[2] &= \begin{cases} (i, 1, 0) & \text{if } (x, y) \text{ falls inside } Q_i \\ \emptyset & \text{otherwise} \end{cases} \end{aligned}$$

The above query can then be realized as:

$$\mathbb{C}_{\text{result}} \leftarrow \mathcal{M}[M_{p'}](\mathcal{B}[\odot](\mathcal{G}[\gamma_d](\mathbb{C}_{\text{origin}}, C_{Q_2}))$$

where

$$\mathbb{C}_{\text{origin}} \leftarrow \mathcal{M}[M_p](\mathcal{B}[\odot](\mathbb{C}_P, C_{Q_1}))$$

is the same expression as the selection query used earlier and selects the points that belong to the intersection between \mathbb{C}_P and C_{Q_1} . The function $\gamma_d : S^3 \rightarrow \mathbb{R}^2$ is used to transform the point from the origin to the destination location and is defined as

$$\forall s \in S^3, \gamma_d(s) = \text{destination}(s[0][0])$$

Here, *destination()* is a function that takes the *id* of the point as input and returns the destination location; and the mask function $M_{p'}$ defined as:

$$M_{p'} = \{s \in S^3 \mid s[0] \neq \emptyset \text{ and } s[2][0] = 2\}$$

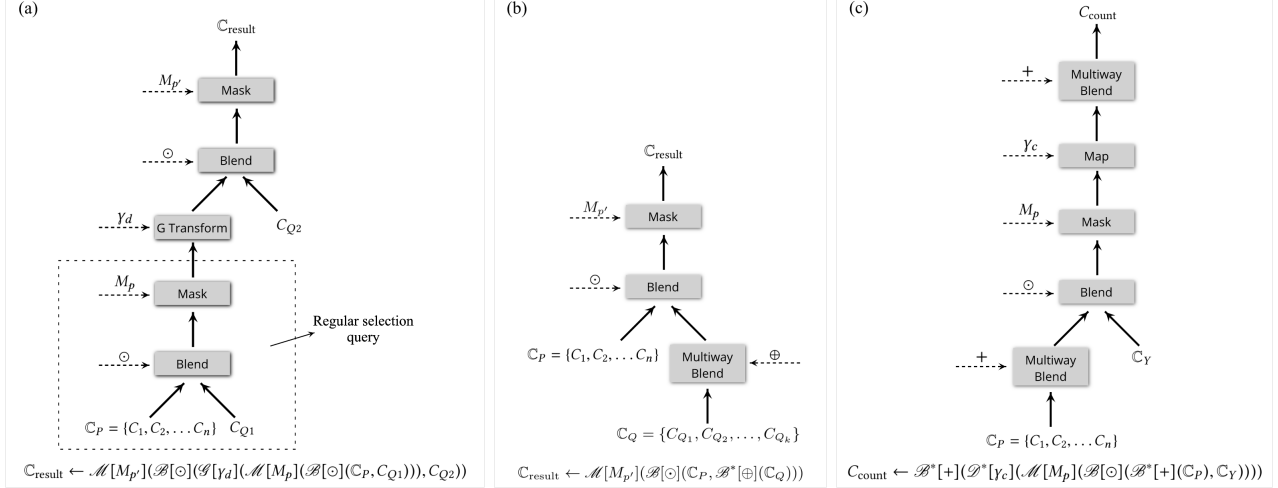


Figure 8: Examples of alternate plan execution strategies for complex queries. (a) Query plan for a selection query over origin-destination data having a polygonal constraint on both spatial attributes. (b) Selection query with multiple polygonal constraints. (c) Spatial aggregation approach used in [47].

The other parameter functions M_p and \odot are defined as before. Figure 8(a) illustrates the above expression as a plan diagram. Intuitively, this plan first computes C_{origin} , i.e., all records whose origin intersect with Q_1 . It then transforms each record in C_{origin} to its destination and tests for their intersection with Q_2 .

5 Notes on Implementation

We now briefly describe a proof-of-concept GPU-based implementation of our model to demonstrate its advantages with respect to enabling the reuse of operators. In particular, we discuss the blend and mask operators required to implement spatial selection queries. To further illustrate the expressive power of our model, we also examine the spatial aggregation operation proposed in [47], and show how it translates directly into an algebraic expression. We note that there can be alternate implementations and that different design choices can be made, but these are beyond the scope of this paper.

5.1 Proof-of-Concept Prototype

The prototype was implemented using C++ and OpenGL. It assumes the traditional representation of point and polygon data sets, that is, they are stored as a set of tuples. Instead of duplicating the geometric objects in the data by explicitly storing the corresponding canvases, we create the canvases on the fly when a query is executed.

Data Representation. Recall from Section 2 that geometric objects are modeled as a union of smooth manifolds, and a canvas representing these objects are defined as a scalar function over \mathbb{R}^2 . Given such a continuous formal representation, it is therefore important to have a discrete representation to be used in the implementation. Our choice was to maintain a canvas as a *texture* [43], which corresponds to a collection of pixels. Here, each pixel stores the object information triple. The canvas functions are defined as discussed in Section 4.1. However, since the pixels discretize the space, it is also necessary to store additional data corresponding to the geometry boundaries. In the case of points, this additional information corresponds to the actual location of the points. For polygons, we store a flag that is set to true if the pixel is on the boundary of the polygon. To accurately identify all boundary pixels, we use an OpenGL extension that enables conservative rasterization. This identifies and draws all pixels that are touched by a triangle (or line), and is different from the default

rasterization, wherein a pixel is only drawn when $> 50\%$ of the pixel is covered by the primitive. This ensures that the border pixels are kept track of in a conservative fashion, and hence there is no loss in accuracy. Additionally, a simple index is maintained that maps each boundary pixel to the actual vector representation of the polygon.

The canvases are created on the fly by simply rendering (i.e., drawing) the geometry using the traditional graphics pipeline. The color components (r,g,b,a) are used to store the canvas function. This rendering is performed onto an off-screen buffer, which generates the required texture. To handle polygons with holes, the outer polygon is first drawn onto the off-screen buffer. The inner polygon (representing one or more holes) is then drawn such that the pixels corresponding to it are negated (i.e., the canvas function is set to null).

Operators. The *blend operator* is accomplished through a straightforward *alpha blending* [43] of two textures, which is supported as part of the graphics pipeline. The *mask operator* looks up each pixel of the texture in parallel and tests for the mask condition. Note that here, the boundary information is used to perform an accurate test if the point is part of a pixel that is on the boundary of the polygon.

Note that if an approximate result suffices, then the hybrid representation of the canvas can be entirely eliminated, making the implementation simpler. In fact, in this case, the texture size can be adjusted in order to appropriately bound the error in the query result, similar to the approach used in [47].

Alternate Implementations. Another possibility for the implementation is to represent geometric objects as a collection of simplicial complexes, thus avoiding any rasterization. The operators then can be implemented to make use of the native ray tracing support provided by the latest RTX-based Nvidia GPUs. We decided to use the rasterization pipeline instead so that our prototype could support any modern GPU from multiple vendors, and not just the RTX GPUs from Nvidia.

Queries. The *polygonal selection of points* is accomplished by first creating the canvases corresponding to the query polygon and query points, which are blended together and then filtered using the mask operator. The operator functions are as defined previously. Our implementation, without any modification, also works for *polygonal selection of polygons*, i.e., if the input is changed from a set of points to a set of polygons.

A straightforward variation of the selection query is to *support multiple polygons as part of the constraint*. In particular, consider the case when the constraint requires the input point to be inside at least one of the polygons (a disjunction). Existing approaches accomplish this by testing the points with respect to each of the polygonal constraints. However, using our model this query can be expressed as follows using just the blend and mask operators:

$$\mathbb{C}_{\text{result}} \leftarrow \mathcal{M}[M_{p'}](\mathcal{B}[\odot](\mathbb{C}_P, \mathcal{B}^*[\oplus](\mathbb{C}_Q)))$$

Here, \mathbb{C}_Q is the collection of canvases corresponding to the query polygons, and \odot and \oplus are the blend functions defined in Section 4.1. The above expression first blends together all the query constraint polygons into a single canvas, which is then used to perform the select similar to the single polygon case. The mask function $M_{p'}$ is defined as:

$$M_{p'} = \{s \in S^3 \mid s[0] \neq \emptyset \text{ and } s[2][0] \geq 1\}$$

Recall that the mask function M_p used for the single query polygon case tests the incidence of the polygon on a pixel by testing the *id* field of the function value corresponding to 2-primitives. Instead, this is accomplished using $M_{p'}$ by checking if the count of the polygons incident on the pixel is at least one. Thus, this mask function $M_{p'}$ is valid even when there is only a single query polygon. So, in our implementation, we use this instead of the M_p defined earlier. Figure 8(b) shows the plan for this query. Furthermore, as we discuss in Section 6, using the proposed operators also helps improve the performance of the queries when compared to the traditional approach. A query with a conjunction can be expressed similarly, by appropriately adjusting the mask function.

5.2 Spatial Aggregation

Consider the spatial join-aggregation query discussed in Section 4.3. Recall that the typical evaluation strategy used by existing systems is to perform a join followed by an aggregation. *RasterJoin* [47] proposed an alternate approach that maps these queries into operations supported by the graphics pipeline in GPUs, leading to orders of magnitude speedup over CPU-based approaches. *RasterJoin* can be directly mapped into a query execution plan using the proposed spatial operators as illustrated in Figure 8(c), and translates to the following expression:

$$C_{\text{count}} \leftarrow \mathcal{B}^*[+](\mathcal{D}^*[\gamma_c](\mathcal{M}[M_p](\mathcal{B}[\odot](\mathcal{B}^*[+](C_P), C_Y))))$$

Here, the parameters $+$, γ_c , M_p , and \odot are the same as defined earlier. While the above expression assumes *count* as the aggregation function, other aggregations can be incorporated by modifying the blend operation parameter $+$ appropriately. Note that in this plan, all the points are first merged into a single canvas which keeps track of partial aggregates. That is, each canvas pixel maintains the count of all points that fall into that pixel. This canvas is then joined with the set of input polygons to identify the points that intersect with the polygons, and the results are again merged to compute the final aggregate. In other words, the counts from the individual pixels that fall within a polygon are combined to generate the aggregation for that polygon. Even though this approach performs an additional merge (through the multiway blend), the size of the input for the join is drastically reduced (there is only one canvas on the left hand side of the blend), thus reducing the cost of the entire plan.

6 Experimental Evaluation

We now briefly discuss the performance of the spatial selection queries using the prototype described above. All experiments were run on a *laptop* having an Intel Core i7-8750H processor, 16 GB memory and 512 GB SSD. The laptop has a dual Nvidia GTX 1070 Max-Q GPU with 8 GB graphics memory, and an integrated Intel UHD Graphics 630 GPU.

Data and Queries. The main goal of our evaluation is to: 1) demonstrate the advantage of using GPU-friendly operators compared to a traditional GPU-based solution; and 2) illustrate how the same operators can be used for variations of a given query. We do this using selection queries that selects trips from the New York City’s taxi data having their pickup location within a query polygon. To demonstrate point (2), we also use queries having a disjunction of multiple polygonal constraints. The size of the input is varied using the pickup time range of the taxi trips.

To mimic real-world use cases, all the query polygons used in these queries were “hand-drawn” using a visual interface (e.g., [16]) and adjusted to have the same MBR. We then use as input only taxi trips that have their pickup location within this MBR. In other words, the evaluation assumes the existence of a filtering stage and primarily focuses on the refinement step. We decided to do this for two reasons. First, the refinement stage, and not filtering, is now the primary bottleneck. Unlike previous decades when the disk-based index filtering was the primary bottleneck, due to the existence of fast ssd-based storage and large CPU memory, the filtering takes only a small fraction of the query time. For example, the filtering step used by the state-of-the-art GPU-based selection approach, even though it is CPU-based, takes only a few milliseconds even for data having over a billion points [11]. Second, when working with complex queries, depending on the query parameters, the optimizer need not always choose to use the spatial index corresponding to a spatial parameter, and the spatial operations could be further up in the plan (e.g., the optimizer might to choose first filter based on another attribute, say time, before performing a spatial operation). In such scenarios, the spatial operation would not have the benefit of an index based filtering, and query bottleneck would then be the refinement step. Additionally, the above setup also helps remove input bias when comparing the performance across polygonal constraints having different shapes and sizes.

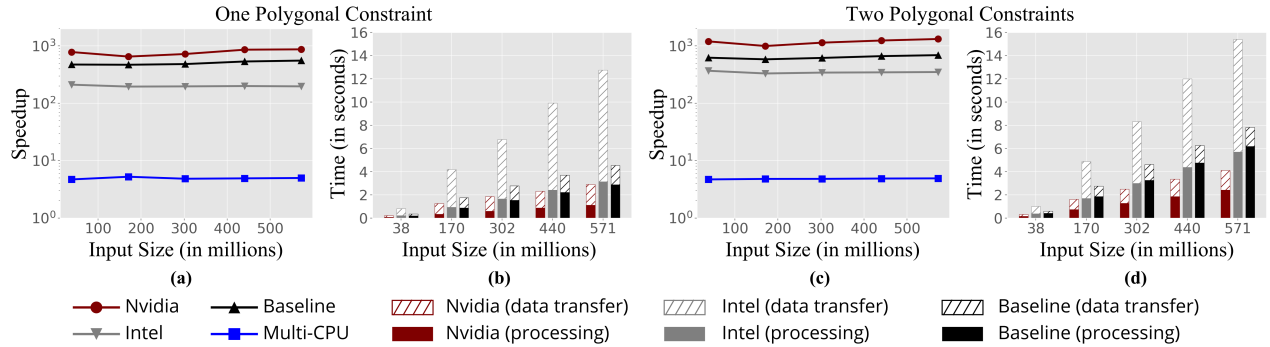


Figure 9: Scaling with input size.

Approaches. We compare the performance of our approach with a CPU baseline, a parallel CPU implementation using OpenMP, as well as a GPU baseline. Because of the above mentioned experimental setup that eliminates the effect of indexes used by current state-of-the-art, we only need to implement the PIP tests for the above baselines. While our approach was executed on two different GPUs (denoted as Nvidia and Intel), the GPU baseline was executed only on the faster Nvidia GPU.

Performance. Figures 9(a) and 9(c) shows the speedup achieved by the different approaches over a single threaded CPU implementation when the query had one and two polygonal constraints, respectively. Note that while all GPU-based approaches are over two orders of magnitude faster than the CPU-based approach, the speedup of our approach increases when the number of polygonal constraint increases. This is because, the only additional work done by our approach when there are additional polygons is to blend the constraint polygons. This is significantly less work when compared to existing approaches which have to perform more PIP tests in this case. This is corroborated when looking at the query run times in Figures 9(b) and 9(d) wherein our approach (in red) requires only 4 seconds (using the Nvidia GPU) even when there are two polygons as constraints even when the query MBR has as many as 571M points. For a given input and GPU, not only is the time to transfer data between the CPU and GPU similar, but is also a significant fraction of the query time. In this light, the speedup in the processing time achieved using our model over a traditional GPU-based approach (which is greater than the overall speedup depicted in Figures 9(a) & (c)) clearly demonstrates the advantages of using a GPU-friendly approach.

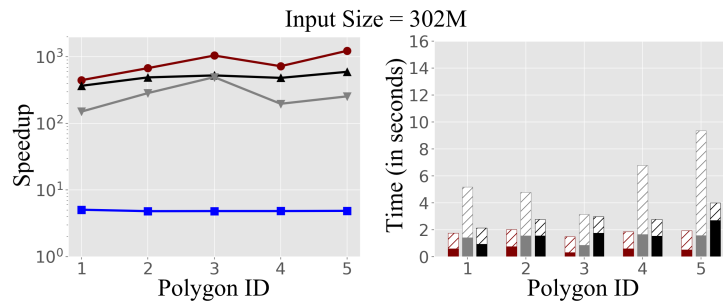


Figure 10: Varying polygonal constraints. Legend is the same as in Figure 9.

Figure 10 shows the speedup and running times when the polygonal constraint is varied. The different polygons had different shapes (and sizes) with query selectivity varying from roughly 3% to 83%. While there is some variation in the processing time depending on the complexity of the polygon constraint, this variation is higher for the baseline. This is because the number of PIP tests performed by the baseline is linearly proportional to the size of the polygon. Irrespective of this complexity, our approach using the discrete GPU requires at most 2 seconds even when the MBR has 302M points.

Also interesting to note is the performance of our approach on the integrated Intel GPU. While, as expected, it is slower than the GPU baseline using a Nvidia GPU, it is still over 2-orders of magnitude faster than the CPU implementation. Given that these GPUs are present in even mid-range laptops, ultrabooks, and even tablets, our algebraic formulation can potentially allow fast spatial queries even on such systems.

7 Discussion

Interoperability with Relational Model. The proposed model is compatible with the relational model and can be incorporated into existing relational systems. Recall that the minimalistic definition of S used in Section 2.2 reserves the first element of the triple to store the unique ID corresponding to the data record. Thus, given a set of canvases corresponding to existing data sets, it is possible to switch to the corresponding relational tuple using this ID. Analogously, the storage structure of a relational tuple can be changed to link to the corresponding canvas, thus allowing connection in the opposite direction. Alternatively, similar to our proof-of-concept implementation, the canvases could also be created on demand.

Thus, conceptually, one can consider the relational tuple and a canvas to be the *dual* of each other allowing a seamless use of the two representations by a query optimizer to appropriately generate query plans involving both spatial and non-spatial operators.

Query Optimization. The proposed model facilitates query optimization in the following ways.

1. *Allowing different query execution plans.* Given a complex query Q , the proposed model enables the creation of multiple plans to realize Q . We gave two such examples in the previous section—one for disjunction and the other for spatial aggregation. In all such scenarios, by appropriately modeling the cost functions of the operators together with metadata about the input, the optimizer can choose a plan that has a lower cost.

2. *Supporting diverse implementations.* It is also possible to have multiple implementations of the same operators, for example, using pre-built spatial indexes. Each of the indexes would result in a different cost based on the properties of the data and the query, thus providing a rich set of options over which to perform the optimization.

3. *Enabling general query processing.* Given the duality between the canvas and the relational tuple as discussed above, the proposed operators can also be easily plugged into existing query optimizers, thus allowing for complex queries involving both the spatial and relational attributes.

Limitations. While the proposed data representation can be directly extended to support 3D primitives, the proposed operators over such 3D data do not have a straightforward implementation using the GPU. Given that native ray tracing support is now being introduced in GPUs, it would be interesting to explore extensions to our algebra that make use of such advances to support 3D spatial queries.

8 Related Work

Spatial Queries. The most common approach used for executing spatial queries is to implement custom techniques for different query types. Selection queries, for example, are typically handled through the use of spatial indexes. These include R-Trees [23], R*-trees [7], kd-trees [8], quad trees [17] and the grid index [40]. While such indexes are also useful for other query types such as spatial joins, enhancements and more efficient algorithms are often designed for specific queries. For instance, several works focus on the filtering step of spatial join algorithms [9, 25, 36, 37]. Custom algorithms have also been designed for spatial aggregation [35, 45, 48, 50] and for nearest neighbor-based queries (see e.g., [24, 26, 28, 41, 52]).

The advent of modern hardware with multiple processing units has led to the design of new approaches that use them for spatial query processing. In particular, GPUs, and clusters supporting the MapReduce paradigm, are extremely popular for this purpose. GPUs have been used for spatial selections [11], spatial

joins [2, 56], spatial aggregations [47], as well as nearest neighbor queries [10, 33]. Similarly, there are dedicated spatial database systems designed using MapReduce such as Hadoop-GIS [3] and Simba [51]. Eldawy and Mokbel [14] provide a comprehensive survey of approaches that use MapReduce for spatial query processing. Covering the numerous work related to different spatial queries is beyond the scope of this paper. However, note that many of these approaches (e.g., indexes) can be easily applied to enhance the operators of the proposed algebra.

Spatial Data Models and Algebras. Specific to spatial databases, Güting [20] introduced geo-relational algebra, which extends relational algebra to include geometric data types and operators. The geometric data types included points, lines, and polygons (without holes) and the geometric operators included operations that are now common in most spatial database solutions (containment, intersection, perimeter, area, etc.). Aref and Samet [5, 6, 42] generalized the above model and provided one of the first high-level discussions on integrating spatial and non-spatial data to build a spatial database system, and the related challenges involved in designing a query optimizer for such a system. Note that current spatial extensions follow approaches very similar to the ideas proposed in these works. This model is *user facing*, i.e., the queries of interest are expressed making use of the data types and the operators provided in the model. The implementation of the operators, however, is left to the developer, and often devolves into having separate implementations for each data type/query combination (similar to the selection query example discussed in Section 1). Our approach, on the other hand, which uses a single representation for all spatial data types and set of GPU-friendly operators different from the traditional operators, is *primarily meant to help database developers implement an efficient GPU-based spatial query engine*: it can be incorporated into existing systems unbeknownst to the user while at the same time providing significant benefits to the database engine and query performance.

Different from the extended relational models, Egenhofer and Franzosa [12] proposed a model that uses concepts from point set topology for spatial queries. In particular, this work models spatial data objects (of a single type, like lines or regions) as closed sets (that defines the underlying topological space), and uses the topological relationship between pairs of closed sets to answer spatial queries. These relationships are computed based on 9 possible intersections computed between the open set, boundary and complement corresponding to the closed sets. Egenhofer and Sharma [13] showed the equivalence of the above model to a raster space, thus making it suitable for GIS queries involving raster data. Kainz et al. [27] model the same topological relations as above, but using partially ordered sets. While theoretically elegant, there are three main shortcomings of this topological approach: (1) the topological relationships are tied to a particular data type, that is, between two regions, or two lines, etc., making it difficult to work with complex spatial objects; (2) computing the relationships requires costly intersection tests to be performed between every pair of spatial objects, making the approach untenable for working with large spatial data sets; and more importantly, (3) while intersection-based queries are straightforward, distance-based queries such as distance-based selections/joins, nearest neighbors etc. cannot be expressed using this model.

Gargano et al. [18] proposed an alternative model that supports complex objects in which spatial objects are represented using a set of rectangular regions. The spatial queries are then realized as operations over these sets. This representation results in a loss of accuracy in the query results. Trying to overcome this using very small rectangles can result in high memory overheads and also require expensive set operations, thus limiting the practical applicability of this model.

Güting and Hartmut proposed another model called Realms [21] and a corresponding ROSE algebra [22]. A Realm models spatial data as a planar graph, where the nodes correspond to points on an integer grid. Given the hardware limitations during that era, the goal of this approach was to avoid costly floating point operations and any imprecision in the query computation. As data is inserted into the database, the spatial objects are “redrawn” to ensure topological consistency (such as locations of intersection points). This framework has important limitations. First, even though the redrawings ensure that queries involving intersection tests can be efficiently and precisely computed using only integer operations, due to the distortion involved, distance-based queries now become imprecise. Second, it is necessary for all query parameters to be a part of the Realm.

Thus, when generating dynamic queries (common in several data analysis tasks), the query parameters have to first be inserted into the Realm, requiring several redrawings of the existing data. Then, after query execution, the newly inserted parameters should be removed. Not only is this expensive, the redrawings caused by the temporary insertions are also not undone, resulting in further distortions. Third, queries involving spatial objects outside the Realm boundaries are not possible. This is a major drawback in modern exploratory data analysis tasks where users can dynamically change their focus as they test and formulate new hypotheses. Finally, similar to the extended relational models, there are separate data types for points, lines, and polygons, making the implementation specific to these data types, and also making it difficult to incorporate complex spatial objects consisting of more than one type.

All of the above models/algebras were designed before GPUs became mainstream, and thus an implementation of these models using GPUs is non-trivial (difficult to parallelize, involves iterative algorithms like intersection computations, etc.). Our approach on the other hand was designed keeping GPUs in mind, and is based on computer graphics operations for which they are optimized.

Models have also been proposed that focus on moving objects [31] which are orthogonal to our work. For GIS applications, Tomlin [46] proposed the Map algebra which was then extended to support time by Jeremy et al. [30]. The map algebra was designed to enable cartographers to easily specify common cartographic functions. Voisard and David [49] propose a layered model specific to geographic maps to help users build new maps. From an implementation point of view, all of the above operations can be translated into spatial queries for execution, and thus an efficient spatial model will be useful in such scenarios as well.

9 Conclusion

In this paper, we introduced a GPU-friendly data model and algebra to support queries over spatial data sets. A key and novel idea in this work is to use a representation that captures the geometric properties inherent in spatial data, and design GPU-friendly operators that can be applied directly on the geometry. We have shown that the proposed algebra is expressive and able to realize common spatial queries. In addition, since the algebra is closed, it can also be used to construct complex queries by composing the operators. The potential ease of implementation afforded by our approach, and its performance even on commodity hardware, can greatly influence the design as well as adoption of GPU-based spatial database solutions, thus democratizing real-time spatial analyses. This is corroborated by the results of the experimental evaluation carried out with our proof-of-concept prototype.

We also believe that this work opens opportunities for new research in the area of spatial query optimization, both for the development of new theory, including algorithms for plan generation and cost estimation, and systems that use the algebra to efficiently evaluate queries over the growing volumes of spatial data.

Acknowledgements

This work was partially supported by the DARPA D3M program and the NYU Moore Sloan Data Science Environment.

References

- [1] D. W. Adler. Db2 spatial extender - spatial data within the rdbms. In *Proc. VLDB*, pages 687–690, San Francisco, CA, USA, 2001. Morgan Kaufmann Publishers Inc.
- [2] D. Aghajarian, S. Puri, and S. Prasad. Gcmf: An efficient end-to-end spatial join system over large polygonal datasets on gpgpu platform. In *Proc. GIS*, pages 18:1–18:10, New York, NY, USA, 2016. ACM.

- [3] A. Aji, F. Wang, H. Vo, R. Lee, Q. Liu, X. Zhang, and J. Saltz. Hadoop gis: A high performance spatial data warehousing system over mapreduce. *PVLDB*, 6(11):1009–1020, Aug. 2013.
- [4] ArcGIS. <https://www.arcgis.com/>, 2018.
- [5] W. G. Aref and H. Samet. Extending a dbms with spatial operations. In *Proc. SSD*, pages 299–318, London, UK, UK, 1991. Springer-Verlag.
- [6] W. G. Aref and H. Samet. Optimization for spatial query processing. In *Proc. VLDB*, pages 81–90, San Francisco, CA, USA, 1991. Morgan Kaufmann Publishers Inc.
- [7] N. Beckmann, H. Kriegel, R. Schneider, and B. Seeger. The r*-tree: an efficient and robust access method for points and rectangles. *SIGMOD Rec.*, 19(2):322–331, May 1990.
- [8] J. L. Bentley. Multidimensional binary search trees used for associative searching. *Commun. ACM*, 18(9):509–517, 1975.
- [9] T. Brinkhoff, H. Kriegel, and B. Seeger. Efficient processing of spatial joins using r-trees. *SIGMOD Rec.*, 22(2):237–246, June 1993.
- [10] B. Bustos, O. Deussen, S. Hiller, and D. Keim. A graphics hardware accelerated algorithm for nearest neighbor search. In V. N. Alexandrov, G. D. van Albada, P. M. A. Sloot, and J. Dongarra, editors, *Proc. ICCS*, pages 196–199, Berlin, Heidelberg, 2006. Springer Berlin Heidelberg.
- [11] H. Doraiswamy, H. T. Vo, C. T. Silva, and J. Freire. A gpu-based index to support interactive spatio-temporal queries over historical data. In *Proc. ICDE*, pages 1086–1097. IEEE, May 2016.
- [12] M. J. Egenhofer and R. D. Franzosa. Point-set topological spatial relations. *Int. J. Geogr. Inf. Syst.*, 5(2):161–174, 1991.
- [13] M. J. Egenhofer and J. Sharma. Topological relations between regions in R^2 and Z^2 . In D. Abel and B. Chin Ooi, editors, *Adv. Spatial Databases*, pages 316–336, Berlin, Heidelberg, 1993. Springer Berlin Heidelberg.
- [14] A. Eldawy and M. F. Mokbel. The era of big spatial data: A survey. *Found. Trends databases*, 6(3-4):163–273, Dec. 2016.
- [15] J.-D. Fekete and C. Silva. Managing Data for Visual Analytics: Opportunities and Challenges. *IEEE Data Eng. Bull.*, 35(3):27–36, 2012.
- [16] N. Ferreira, J. Poco, H. T. Vo, J. Freire, and C. T. Silva. Visual exploration of big spatio-temporal urban data: A study of new york city taxi trips. *IEEE TVCG*, 19(12):2149–2158, 2013.
- [17] R. Finkel and J. Bentley. Quad trees a data structure for retrieval on composite keys. *Acta Informatica*, 4(1):1–9, 1974.
- [18] M. Gargano, E. Nardelli, and M. Talamo. Abstract data types for the logical modeling of complex data. *Information Systems*, 16(6):565 – 583, 1991.
- [19] GRASS GIS. <https://grass.osgeo.org/>, 2018.
- [20] R. H. Güting. Geo-relational algebra: A model and query language for geometric database systems. In *Proc. EDBT*, pages 506–527, London, UK, UK, 1988. Springer-Verlag.

- [21] R. H. Güting and M. Schneider. Realms: A foundation for spatial data types in database systems. In D. Abel and B. Chin Ooi, editors, *Adv. Spatial Databases*, pages 14–35, Berlin, Heidelberg, 1993. Springer Berlin Heidelberg.
- [22] R. H. Güting and M. Schneider. Realm-based spatial data types: The rose algebra. *VLDBJ*, 4(2):243–286, Apr 1995.
- [23] A. Guttman. R-trees: a dynamic index structure for spatial searching. *SIGMOD Rec.*, 14(2):47–57, June 1984.
- [24] G. R. Hjaltason and H. Samet. Distance browsing in spatial databases. *ACM Trans. Database Syst.*, 24(2):265–318, June 1999.
- [25] E. H. Jacox and H. Samet. Spatial join techniques. *ACM Trans. Database Syst.*, 32(1), Mar. 2007.
- [26] H. V. Jagadish, B. C. Ooi, K. Tan, C. Yu, and R. Zhang. idistance: An adaptive b+-tree based indexing method for nearest neighbor search. *ACM Trans. Database Syst.*, 30(2):364–397, June 2005.
- [27] W. Kainz, M. J. Egenhofer, and I. Greasley. Modelling spatial relations and operations with partially ordered sets. *Int. J. Geogr. Inf. Syst.*, 7(3):215–229, 1993.
- [28] N. Katayama and S. Satoh. The sr-tree: An index structure for high-dimensional nearest neighbor queries. *SIGMOD Rec.*, 26(2):369–380, June 1997.
- [29] Z. Liu and J. Heer. The effects of interactive latency on exploratory visual analysis. *IEEE TVCG*, 20(12):2122–2131, 2014.
- [30] J. M., R. V., and C. D. Tomlin. Cubic map algebra functions for spatio-temporal analysis. *CaGIS*, 32(1):17–32, 2005.
- [31] J. K. Nidzwetzki and R. H. Güting. Distributed secondo: an extensible and scalable database management system. *Distributed and Parallel Databases*, 35(3):197–248, Dec 2017.
- [32] Oracle Spatial and Graph. <https://www.oracle.com/technetwork/database-options/spatialandgraph/documentation/spatial-doc-idx-161760.html>, 2018.
- [33] J. Pan and D. Manocha. Fast gpu-based locality sensitive hashing for k-nearest neighbor computation. In *Proc. GIS*, pages 211–220, New York, NY, USA, 2011. ACM.
- [34] V. Pandey, A. Kipf, T. Neumann, and A. Kemper. How good are modern spatial analytics systems? *PVLDB*, 11(11):1661–1673, July 2018.
- [35] D. Papadias, P. Kalnis, J. Zhang, and Y. Tao. Efficient olap operations in spatial data warehouses. In *Proc. SSTD*, pages 443–459, London, UK, UK, 2001. Springer-Verlag.
- [36] J. Patel and D. DeWitt. Partition based spatial-merge join. *SIGMOD Rec.*, 25(2):259–270, June 1996.
- [37] M. Pavlovic, T. Heinis, F. Tauheed, P. Karras, and A. Ailamaki. Transformers: Robust spatial joins on non-uniform data distributions. In *Proc. ICDE*, pages 673–684. IEEE, May 2016.
- [38] PostGIS: Spatial and geographic objects for PostgreSQL. <http://postgis.net>, 2018.
- [39] QGIS. <https://www.qgis.org/en/site/>, 2018.

- [40] P. Rigaux, M. Scholl, and A. Voisard. *Spatial Databases with Application to GIS*. Morgan Kaufmann Publishers Inc., San Francisco, CA, USA, 2002.
- [41] N. Roussopoulos, S. Kelley, and F. Vincent. Nearest neighbor queries. *SIGMOD Rec.*, 24(2):71–79, May 1995.
- [42] H. Samet and W. G. Aref. Spatial data models and query processing. In W. Kim, editor, *Modern Database Systems*, pages 338–360. ACM Press/Addison-Wesley Publishing Co., New York, NY, USA, 1995.
- [43] D. Shreiner, G. Sellers, J. M. Kessenich, and B. M. Licea-Kane. *OpenGL Programming Guide: The Official Guide to Learning OpenGL, Version 4.3*. Addison-Wesley Professional, 8th edition, 2013.
- [44] SQL Server Spatial. <https://docs.microsoft.com/en-us/sql/relational-databases/spatial/spatial-data-sql-server?view=sql-server-2017>, 2018.
- [45] Y. Tao, D. Papadias, and J. Zhang. Aggregate processing of planar points. In *Proc. EDBT*, pages 682–700, Berlin, Heidelberg, 2002. Springer Berlin Heidelberg.
- [46] C. D. Tomlin. Map algebra: one perspective. *Landscape and Urban Planning*, 30(1-2):3–12, 1994.
- [47] E. Tzirita Zacharitou, H. Doraiswamy, A. Ailamaki, C. T. Silva, and J. Freire. Gpu rasterization for real-time spatial aggregation over arbitrary polygons. *PVLDB*, 11(3):352–365, 2017.
- [48] I. F. V. Lopez, R. T. Snodgrass, and B. Moon. Spatiotemporal aggregate computation: A survey. *IEEE TKDE*, 17(2):271–286, Feb. 2005.
- [49] A. Voisard and B. David. A database perspective on geospatial data modeling. *IEEE TKDE*, 14(2):226–243, March 2002.
- [50] L. Wang, R. Christensen, F. Li, and K. Yi. Spatial online sampling and aggregation. *PVLDB*, 9(3):84–95, 2015.
- [51] D. Xie, F. Li, B. Yao, G. Li, L. Zhou, and M. Guo. Simba: Efficient in-memory spatial analytics. In *Proc. SIGMOD*, pages 1071–1085, New York, NY, USA, 2016. ACM.
- [52] P. N. Yianilos. Data structures and algorithms for nearest neighbor search in general metric spaces. In *Proc. SODA*, pages 311–321, Philadelphia, PA, USA, 1993. Society for Industrial and Applied Mathematics.
- [53] J. Zhang and S. You. Speeding up large-scale point-in-polygon test based spatial join on gpus. In *Proc. BigSpatial*, pages 23–32, 2012.
- [54] J. Zhang, S. You, and L. Gruenwald. High-performance online spatial and temporal aggregations on multi-core cpus and many-core gpus. In *Proc. DOLAP*, pages 89–96, 2012.
- [55] J. Zhang, S. You, and L. Gruenwald. High-performance spatial join processing on gpgpus with applications to large-scale taxi trip data. Technical report, The City College of New York, 2012.
- [56] J. Zhang, S. You, and L. Gruenwald. Efficient parallel zonal statistics on large-scale global biodiversity data on gpus. In *Proc. BigSpatial*, pages 35–44, New York, NY, USA, 2015. ACM.